Environment International 202 (2025) 109615

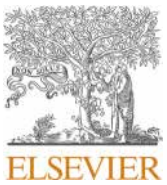

Contents lists available at ScienceDirect

Environment International

journal homepage: www.elsevier.com/locate/envint

Full length article

High-resolution modelling of particulate matter chemical composition over Europe: brake wear pollution

Abhishek Upadhyay [a,*], Jianhui Jiang [b], Yun Cheng [c], Petros Vasilakos [a], Ying Chen [d], Daniel Trejo Banos [c], Benjamin Flückiger [e,f], Manousos I. Manousakas [a], André S.H. Prévôt [a], Robin L. Modini [a], Ana Sánchez de la Campa [g], Andrea Schemmel [h], Andrés Alastuey [i], Benjamin Bergmans [j], Célia A. Alves [k], Christoph Hueglin [l], Cristina Colombi [m], Cristina Reche [i], Daniel Sánchez-Rodas [g], Dario Massabò [n,o], Evangelia Diapouli [p], Federico Mazzei [n,o], Franco Lucarelli [q,r], Gaëlle Uzu [s], Imre Salma [t], Jean-Luc Jaffrezo [s], Jesús D. de la Rosa [g], Jolanda E. Reusser [u,v,w], Kostas Eleftheriadis [p], Laurent Y. Alleman [x,y], Mark Scerri [z], Mirko Severi [aa], Olivier Favez [ab,x], Paolo Prati [n,o], Rita Traversi [aa], Roberta Vecchi [ac], Silvia Becagli [aa], Silvia Nava [r,s], Sonia Castillo [ad], Sophie Darfeuil [s], Stuart K. Grange [l,ae], Xavier Querol [i], Zsófia Kertész [af], Giancarlo Ciarelli [ag], Nicole Probst-Hensch [d,e], Danielle Vienneau [d,e], Jeroen Kuenen [ah], Hugo Denier Van Der Gon [ah], Kaspar R. Daellenbach [a,*], Ekaterina Krymova [c], Kees de Hoogh [e,f,**], Imad El-Haddad [a,ai,***]

[a] PSI Center for Energy and Environmental Sciences, 5232 Villigen PSI, Switzerland
[b] Global Institute for Urban and Regional Sustainability, School of Ecological and Environmental Sciences, East China Normal University, 200241 Shanghai, China
[c] Swiss Data Science Center, EPFL and ETH Zürich, Zürich, Switzerland
[d] School of Geography, Earth and Environmental Sciences, University of Birmingham, Edgbaston, Birmingham B15 2TT, United Kingdom
[e] Swiss Tropical and Public Health Institute Swiss TPH, Allschwil, Switzerland
[f] University of Basel, P.O. Box, CH-4003 Basel, Switzerland
[g] CIQSO-Center for Research in Sustainable Chemistry, Associate Unit CSIC-University of Huelva "Atmospheric Pollution", Campus El Carmen s/n, 21071 Huelva, Spain
[h] Federal Environment Agency, Germany
[i] Institute of Environmental Assessment and Water Research (IDAEA-CSIC), Barcelona, Spain
[j] Institut Scientifique de Service Public – ISSeP, Belgium
[k] Department of Environment and Planning, CESAM – Centre for Environmental and Marine Studies, University of Aveiro 3810-193 Aveiro, Portugal
[l] Empa, Swiss Federal Laboratories for Materials Science and Technology, 8600 Dübendorf, Switzerland
[m] Agenzia Regionale per la Protezione dell'Ambiente Lombardia (ARPA Lombardia), 20124 Milan, Italy
[n] Dipartimento di Fisica, Università di Genova, via Dodecaneso 33, 16146 Genova, Italy
[o] National Institute of Nuclear Physics (INFN) – Division of Genoa, via Dodecaneso 33, 16146 Genova, Italy
[p] Institute of Nuclear & Radiological Sciences & Technology, Energy & Safety, N.C.S.R. "Demokritos", Athens 15310, Greece
[q] Department of Physics and Astronomy, University of Florence, Sesto Fiorentino, 50019 Florence, Italy
[r] National Institute of Nuclear Physics (INFN), Sesto Fiorentino, 50019 Florence, Italy
[s] University Grenoble Alpes, CNRS, IRD, INP-G, INRAE, IGE (UMR 5001), 38000 Grenoble, France
[t] Institute of Chemistry, Eötvös Loránd University, Hungary
[u] Department of Environmental Systems Science, ETH Zurich, CH-8092 Zürich, Switzerland
[v] Swiss Federal Institute of Aquatic Science and Technology (Eawag), CH-8600 Dübendorf, Switzerland
[w] Agroecology and Environment, Agroscope, CH-8046 Zurich, Switzerland
[x] Laboratoire Central de Surveillance de la Qualité de l'air (LCSQA), Verneuil-en-Halatte F-60550, France
[y] IMT Nord Europe, Institut Mines-Télécom, Université de Lille, Centre for Energy and Environnement, 59000 Lille, France
[z] Institute of Earth Systems, University of Malta, Msida MSD2080, Malta
[aa] Department of Chemistry "Ugo Schiff", University of Florence, 50019 Sesto F.no (Florence), Italy

* Corresponding author.
** Corresponding author at: Swiss Tropical and Public Health Institute Swiss TPH, Allschwil, Switzerland.
*** Corresponding author at: PSI Center for Energy and Environmental Sciences, 5232 Villigen PSI, Switzerland.
E-mail addresses: abhishek.upadhyay@psi.ch (A. Upadhyay), kaspar.daellenbach@psi.ch (K.R. Daellenbach), c.dehoogh@swisstph.ch (K. de Hoogh), imad.el-haddad@psi.ch (I. El-Haddad).

https://doi.org/10.1016/j.envint.2025.109615
Received 12 March 2025; Received in revised form 28 May 2025; Accepted 16 June 2025
Available online 22 June 2025

[ab] INERIS, Parc Technol. ALATA, Verneuil-en-Hala 60550, France
[ac] Department of Physics, Università degli Studi di Milano, Milan 20133, Italy
[ad] Department of Applied Physics, Universidad de Granada, Av. de la Fuente Nueva, 18071 Granada, Spain
[ae] School of Earth and Atmospheric Sciences, Queensland University of Technology, Gardens Point, Brisbane, Queensland 4000, Australia
[af] Laboratory for Heritage Science, HUN-REN Institute for Nuclear Research, Debrecen, Hungary
[ag] Institute for Atmospheric and Earth System Research/Physics, Faculty of Science, University of Helsinki, Finland
[ah] TNO, Department of Air Quality & Emission Research, Princetonlaan 6, 3584 CB Utrecht, the Netherlands
[ai] College of Environmental Sciences and Engineering, Peking University, Beijing, China

ARTICLE INFO

Handling Editor: Dr. Hanna Boogaard

Keywords:
Brake wear
Non-exhaust emissions
Atmospheric Cu
Copper
CAMx
Random forest

ABSTRACT

In today's rapidly evolving society, the sources of atmospheric particulate matter (PM) emissions are shifting significantly. Stringent regulations on vehicle tailpipe emissions, in combination with a lack of control of non-exhaust vehicular emissions, have led to an increase in the relative contribution of non-exhaust PM in Europe. This study analyzes the spatial distribution, temporal trends, and impacts of brake wear PM pollution across Europe by modeling copper (Cu) concentrations at a high spatial resolution of ~250 m which is a key tracer of brake-wear emissions. We integrated coarse-resolution brake-wear Cu from CAMx chemical transport model and high-resolution land use data into a random forest (RF) model to predict Cu concentrations at ~250 m over whole of continental Europe. The RF model was trained using an unprecedented dataset of over 50,000 daily Cu measurements from 152 sites. It corrected CAMx underestimation and downscaled Cu to a higher spatial resolution. In validation, the model showed robust spatial and temporal prediction with good Pearson's correlation coefficients of 0.6 and 0.7, respectively. We generated 10 years (2010–2019) of daily Cu concentrations over Europe, revealing spatial patterns aligned with urbanization and road networks, with peaks in cities and lower values in rural areas. Temporal trends reveal that Cu concentrations generally peak on weekdays and in winter. Despite a decline in PM across Europe over decades, Cu concentrations showed no decrease in many cities from 2010 to 2019. Cu levels are strongly correlated with population density with more than 12 million Europeans exposed to levels exceeding 40 ng/m^3, equivalent to around 1 μg/m^3 of total PM_{10} from brake wear. Our findings highlight the need for expanded metal measurement for non-exhaust tracers for a better understanding of the health relevance of PM composition including Cu, and more effective regulations of non-exhaust PM emissions as included in EURO 7 vehicles.

1. Introduction

Air pollution poses a threat to human health and climate. The expansion of the mobility sector, driven by rapid economic growth and urban development, has resulted in a notable increase in vehicular emissions. Motor vehicles contribute to air pollution through exhaust as well as non-exhaust emissions. Exhaust emissions stem from fuel combustion, while non-exhaust emissions arise from brake wear, tire wear, road surface wear, resuspended particles from road dust, and volatile organic compounds (VOCs) from fuel evaporation and vehicle maintenance (Harrison et al., 2021; Johansson et al., 2009). Over the past few decades, regulations have significantly reduced exhaust emissions. However, non-exhaust emissions remain largely unregulated, causing their relative contribution to total vehicular pollution to grow (Gon and Der, 2013; Harrison et al., 2021; Salma and Maenhaut, 2006; Thorpe and Harrison, 2008). Additionally, non-exhaust emissions are also increasing because of the continuous rise in the number of vehicles. Electric vehicles (EVs), while reducing gaseous and particulate matter (PM) exhaust emissions, do not address overall on-road vehicular pollution since non-exhaust PM emissions are proportional to vehicle weight, and EVs tend to be heavier than vehicles with internal combustion engines by around 20–25% (Timmers and Achten, 2016; Woo et al., 2022). As a result, PM emissions from EVs and modern combustion vehicles are now nearly comparable (Timmers and Achten, 2016). Material abrasion in non-exhaust processes mainly produces larger particles, which can be adequately expressed and assessed by their mass concentration. Understanding the sources, contributions, trends, and health impact of non-exhaust pollution is essential to inform effective regulatory measures for reducing these emissions, as for the first-time regulation of PM_{10} emissions from brakes is included in the EURO 7 emission standard by European Union (EU) (Council of the EU, 2024). In previous regulations on brake wear, the EU implemented stringent measures to eliminate asbestos-containing materials decades ago, leading to the widespread use of asbestos-free brake linings across Europe (European Union, 1999). Abrasions from brake pads release non-exhaust particles rich in potentially toxic metals such as Fe, Cu, Sb, Ba, Sn, and Mn, with sizes ranging from ~100 nm to ~10 μm, although the prevalent mass contribution falls in the range of 2.5–10 μm (Thorpe and Harrison, 2008). Although Cu is majorly emitted by transportation, industrial and energy sectors, 70–90% of Cu near traffic sources and city centers come from brake wear emissions, suggesting, Cu can serve as a reliable tracer for non-exhaust emissions (Charron et al., 2019; Denier van der Gon et al., 2007; Johansson et al., 2009; Salma and Maenhaut, 2006; Thorpe and Harrison, 2008). In addition, Cu, known for its high intrinsic oxidative potential has been linked to adverse health outcomes due to its ability to generate reactive oxygen species, which can promote immune disorders, metabolic diseases, and genetic damage (Fussell et al., 2022; Rodopoulou et al., 2022; Schiavo et al., 2023). Epidemiological studies have shown a 6.3% increase in the inflammatory blood markers high-sensitivity C-reactive protein (hsCRP) with 5 ng/m^3 increase in $PM_{2.5}$ copper using European cohorts (Hampel et al., 2015). However, epidemiological studies on non-exhaust PM pollution are limited due to the lack of exposure data (Beelen et al., 2015; Chen et al., 2021; Fussell et al., 2022).

Non-exhaust PM tends to exhibit considerable spatial variability due to their coarse mode size, with elevated concentrations often observed near high-traffic intersections and residential areas. This underscores the need for detailed, high spatial resolution Cu concentration data to inform exposure assessments. While metal measurements at specific sites provide valuable information, they are insufficient for exposure assessment, due to limited spatial coverage. Chemical transport models (CTMs) can produce spatially and temporally continuous maps of pollutants, but the high spatial resolution required for accurate exposure estimates is computationally challenging. In addition, inventories dedicated to brake wear emissions are rare. Land use regression models, which are typically used for high-resolution air pollution modeling, require high-density observation data for accurate predictions. Recently, the use of machine learning models has been instrumental in improving the predictions of different chemical transport models, including LOTOS-EUROS (Xu et al., 2021), GEOS-Chem (Ivatt and Evans, 2020),

Copernicus Atmosphere Monitoring Service (CAMS) (Bertrand et al., 2023), WRF-Chem (Han et al., 2023), CMAQ (Sayeed et al., 2022), CHIMERE (Chelhaoui et al., 2024) and CAMx (Hosseinpour et al., 2024), and downscaling (Jianyao et al., 2025). Hybrid methods have emerged, integrating CTMs' ability to simulate atmospheric dynamics with land use data for enhanced spatial resolution too (de Hoogh et al., 2018). These hybrid models can correct biases and downscale pure CTM outputs, thus bridging the gap in fine-resolution non-exhaust emission modeling.

This study presents the first hybrid model for predicting daily mean Cu concentrations from brake wear for the European domain, at a ~ 250 × 250 m resolution over the years 2010–2019. We have integrated a unique brake wear emission inventory in a CTM to generate ~12 km × 12 km resolution maps of Cu concentrations. These maps were then downscaled using a random forest model incorporating fine-resolution land use information. The model was trained on an unprecedented observational data set of over 50,000 daily Cu concentrations from 152 European sites. The model outputs enable analysis of both spatial and temporal trends in brake wear emissions, and they are suitable for exposure assessment needed to support epidemiological and health impact studies.

2. Methodology

2.1. CAMx model for Cu modelling at a coarser spatial resolution

We used the Comprehensive Air Quality Model with extensions (CAMx) version 6.5 to simulate hourly fine and coarse mode Cu concentrations. The simulation used inert aerosol treatment (with the aerosol option "INERT") where it accounts for transport, dispersion, and deposition processes while excluding chemical reactions (ENVIRON, 2018). The simulation domain covers Europe with 200 longitudinal and 280 latitudinal grid points, at a spatial resolution of 0.25° × 0.125° and 14 vertical layers extending to 100 hPa, which includes elevations ranging from ~20 to 7000 m above sea level. CAMx was run offline, using the Weather Research and Forecasting (WRF) meteorology and emissions based on CAMS-REG-v4.2 (Kuenen et al., 2022) prepared by the Netherlands Organisation for Applied Scientific Research (TNO) as inputs. Meteorological parameters were simulated for the specified domain and resolution with a three-day spin-up, using ERA5 data for initial and boundary conditions. The similar model setup is validated with ground-based observations for meteorological parameters like temperature, wind speed, and wind direction and chemical parameters like organic aerosol (OA) in the previous studies from our group and show good model performance (Jiang et al., 2019a,b). The multi-year emission inventory for vehicular wear Cu used in this setup was generated, combining emissions from the COPERT model (EMISIA, 2020) for vehicle emissions with a spatial distribution using the same methodologies as for the CAMS-REG emission inventories (Kuenen et al., 2022). The brake wear emission inventory includes emissions from motorcycles, passenger cars, light-duty vehicles, and heavy-duty vehicles. It considers emissions in different traffic patterns like driving in urban areas, on highways, and on rural roads (Denier van der Gon et al., 2018). The chemical composition of brake wear is based on elemental composition analysis of braking materials (Hulskotte et al., 2014). The CAMx simulations spanned a decade (2010–2019), providing hourly Cu concentration estimates across Europe to capture long-term trends.

2.2. Random forest model for improved prediction and spatial downscaling

Random forest (RF) is a machine learning algorithm that employs an ensemble of decision trees to model complex, non-linear relationships between predictors and target variables (Hu et al., 2017; Breiman, 2001; Chen et al., 2019). We applied RF to downscale CAMx outputs to ~ 250 m spatial resolution and to improve the prediction accuracy as well. To do this, we modelled the logarithmic ratio of ground-based Cu observations to CAMx-simulated Cu as the target variable, thus correcting CAMx biases due to emission uncertainties, potentially missing sources like resuspended particles, and coarser resolution. Using CAMx concentration as input to RF model instead of ratio led the model to create a sharp distinction between low and high CAMx values, producing two separate distributions of predictions. Within each range, the model exhibited an almost flat response relative to the observations, resulting in unsatisfactory performance and limited predictive power, in contrast, the ratio captures variability better as discussed in the result section. The logarithmic transformation of observed to CAMx ratio allows covering the large dynamic range in this ratio and ensures stable model performance (consistent precision and accuracy) across the full range of copper concentrations. Although Cu is also emitted from sources such as manufacturing and extractive industries (including Cu smelters) and railway and tram transportation, brake wear emissions are the dominant contributor. Emission from the road transport sector accounts for ~70–90 % of total Cu in European countries (CITEPA, 2018; EEA-Report, 2024). While the observed Cu includes contributions from all sources, we assume that the modeled Cu primarily represents brake wear emissions. Here, the key modeling component, CAMx simulations, aligns with this assumption by specifically simulating Cu concentrations from brake wear. The RF predictors included land use variables and major meteorological parameters. The use of high-resolution land use data (at scales ranging from 25 m to 1 km) enables the RF model to produce bias-corrected daily Cu concentration maps across Europe at a fine spatial scale. The model operates at a daily temporal resolution, allowing us to distinguish the effects of land use, activity, and meteorological variations more effectively, resulting in a more robust predictive capability in both space and time.

We used meteorological parameters from WRF simulation as predictors to the RF model including ambient temperature (at 2 m height), relative humidity, planetary boundary layer height (PBLH), wind speed (at 10 m height), and atmospheric surface pressure. Land use predictors were sourced from multiple databases, as summarized in Table S1. They include the fraction of different land use types (e.g., agricultural, industrial, natural green, barren land), road network lengths, percentage of buildup area represented by impervious surface density (IMD), and elevation. In addition, we have also used Cu concentration in topsoil, population density, day of the week, and month of the year as predictor variables. The data on Cu concentration in topsoil were sourced from the European Soil Data Centre (ESDAC) for the European Union (Panagos et al., 2022), and for Switzerland, it was obtained from the Swiss Centre of Excellence for Agricultural Research Agroscope (Reusser, 2023). These predictors are correlated with Cu as well as with one another. For a detailed overview of these correlations, please refer to the correlation clusters heatmap in Fig. S12. We applied bilinear interpolation to resample all required CAMx and WRF variables to a finer spatial resolution of ~ 250 m. Similarly, all required land-use variables were regridded to this ~250 m resolution from initial resolutions varying from 25 m to 1000 m. Subsequently, the Point location data for training and validation were extracted from the interpolated datasets.

To train our model, we used the most comprehensive ground-based dataset of Cu concentrations in PM_{10} fraction in Europe, comprising 152 monitoring stations and totaling more than 50,000 daily data points (Fig. 1). Table S2 summarizes monitoring locations with metal measurement methodology for each location. In brief, the most used measurement techniques are Inductively Coupled Plasma Mass Spectrometry (ICP-MS), X-ray fluorescence (XRF) spectrometry, and particle-induced X-ray emission (PIXE) spectrometry. ICP-MS is based on the digestion and analysis of a sample whereas PIXE and XRF (including the Xact instrument) are both non-destructive, X-ray-based nuclear techniques. Multiple aerosol studies have demonstrated strong agreement between PIXE and XRF for elemental concentrations, including Cu. For instance, Gini et al. (2021) conducted an inter-laboratory comparison of PM_{10} samples analyzed by both PIXE and

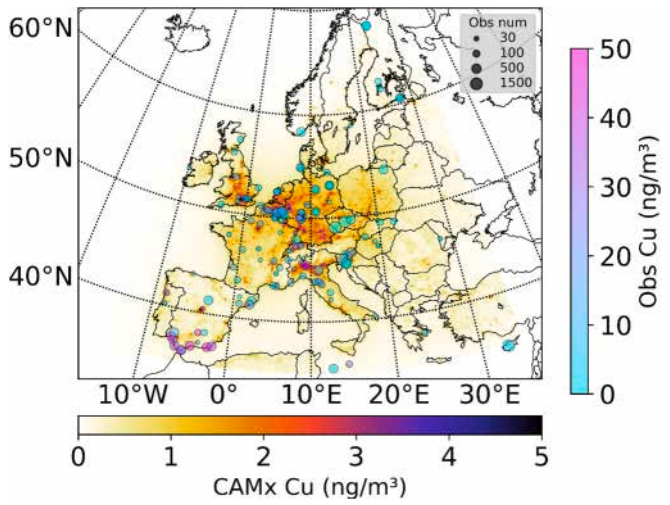

Fig. 1. Spatial distribution of CAMx simulated multi-year (2010–2019) mean Cu concentration across Europe and mean observed Cu concentration from ground-based monitoring sites represented by the markers scattered over the map. The color of the markers represents the mean concentration at the monitoring location and the size of the markers represents the number of data points available at locations.

XRF and found excellent consistency for Cu among other elements, with differences typically below 10 %. Similarly, Chiari et al. (2018) and Lucarelli et al. (2011) support the reliability and interchangeability of PIXE and XRF in aerosol applications. While ICP-MS is fundamentally different compared to PIXE and XRF, studies have shown very good agreement for trace metals like Cu. A study by Saitoh et al. (2002) comparing ICP-MS and PIXE measurements on PM_{10} samples reported correlation coefficients (R^2) above 0.9 for most metals, including Cu. These validate the cross-comparability of the methods for this specific analyte and we consider the Cu data from PIXE, XRF, and ICP-MS in this study to be directly comparable and compatible with our modelling framework. The average error in determining Cu concentration is ~10%, which is far lower than the uncertainties of our model (~30–50%) and more than 95% of the data are 5 times higher than detection limits. Therefore, we have not considered the measurement errors in the modelling framework.

Table S2 also details the number of observations and corresponding mean concentrations for each site. Given the heterogeneity of PM chemical composition measurements across Europe, data were gathered through scientific collaborations, regional air quality networks, and government agencies to ensure the most comprehensive and accurate dataset. This database is part of a larger initiative to develop a global dataset on PM chemical composition (El Haddad et al., 2024).

We conducted a hyperparameter search to obtain an optimized model using cross-validation to determine the optimal combination of the hyperparameters of RandomForestRegressor from the *scikit-learn* library of Python (Pedregosa et al., 2011). This included optimization for the number of trees in the RF ensemble, the maximum number of features to consider when looking for the best split, the minimum number of samples required to split a node, and the maximum depth of the tree. To evaluate the prediction quality on the held-out splits, we used the squared error criterion. The optimal hyperparameters obtained from tuning for the final model were determined as follows: the "n_estimators" was 300, the "maximum_features" was 0.5, the "minimum_samples_split" was 2, and the maximum_depth was 25. We thoroughly validated the model using different approaches to develop a spatially and temporally robust model. Spatial robustness was assessed by performing validations on unseen locations, where 10 % of the locations were held out for validation in iteration, and performed 10 iterations to ensure a comprehensive evaluation for all locations. Temporal consistency was checked through a leave-one-year-out validation. To ascertain the impact of CAMx, we trained and validated another RF model, without anchoring it to the CAMx Cu results. In addition to the training and validation statistics, we conducted an in-depth analysis of the predicted Cu maps to identify and rectify any unusual patterns like the impact of road variable in different buffer sizes. We used CAMx, WRF, and LU dataset rescaled to uniform 250 m resolution as input for the RF model while facilitating predictions across the entire domain. This approach ensures consistency during the model development and prediction.

2.3 Assumptions and limitations

In this study, we assume that total Cu concentrations reflect brake wear emissions. Copper is widely recognized as a reliable tracer for vehicular brake wear, as supported by numerous modelling and observational studies (Charron et al., 2019; Denier van der Gon et al., 2007; Johansson et al., 2009; Salma and Maenhaut, 2006; Thorpe and Harrison, 2008). For example, over 90 % of Cu in Stockholm air has been attributed to traffic emissions, mainly from brake wear (Johansson et al., 2009); similar contributions have been reported in Birmingham (97 %; Birmili et al., 2006), Budapest (69 %; Salma and Maenhaut, 2006), and São Leopoldo and Canoas, Brazil (81 %; Alves et al., 2020). Our analysis supports these findings. Observed Cu concentrations correlate well with total road length within a 1000 m buffer (Pearson's r = 0.49; Fig. S1a), a relationship comparable to that between observed and CAMx-simulated Cu (Pearson's r = 0.45; Fig. S1b), which is based on brake wear emission inventories. Additionally, observed Cu levels exhibit a strong correlation with CAMx-simulated nitrogen oxides (NO_x) (r = 0.55; Fig. S2a), a well-established tracer for exhaust traffic pollutant. CAMx-predictions of Cu and NO_x themselves are highly correlated (r = 0.89), reinforcing their shared traffic-related origin. While the other sources of Cu such as metal smelting exist, these are typically spatially localized and not dominant in traffic-heavy environments. To our knowledge, the monitoring sites included in our analysis are not located near major industrial Cu sources. As shall be discussed below, the RF bias correction and downscaling largely follow road density and urban land use, with negligible influence from industrial area coverage. This supports the interpretation that RF-CAMx Cu predictions primarily represent traffic-related brake wear emissions.

Another limitation of our approach is that atmospheric dispersion is not explicitly simulated at the high resolution (~250 m) of the downscaled outputs. Instead, concentrations in adjacent high-resolution grid cells are estimated independently. That is, while CAMx simulates transport, dispersion and deposition at a coarse resolution of ~12 km, high resolution land-use variables combined with coarse resolution meteorology are used to bias-correct and downscale CAMx outputs to ~250 m resolution. Despite this, we do not observe significant discontinuities in the predicted Cu concentration fields (see Figures 2b and 3a). Methods that account for spatial autocorrelation, such as kriging, do exist, but they require a much denser observational network than is currently available to be effective (Chen et al., 2019; Wong et al., 2021).

As noted above, analytical uncertainties in Cu measurements are relatively minor compared to other sources of error. However, temporal coverage varied across sites, with some offering few months of data and others spanning multiple years. However, our analysis shows that increasing the number of sites in the training set improves model performance more than extending the time series. Therefore, we prioritized the inclusion of more sites, even when their time series were relatively short. The data used were not collected through a unified campaign designed for the purpose of the study but stemmed from independent efforts across Europe over the past decade. This approach enabled us to build on the most comprehensive aerosol elemental composition dataset to date, while also underscoring the need for more coordinated, long-term, multi-site measurements across the continent. On the modelling side, uncertainties arise from the representation of meteorological

conditions, transport, and deposition processes. These are influenced by assumptions in model parameterizations and the coarse spatial resolution, both of which can limit the accuracy in simulating pollutant dispersion. Additionally, uncertainties in emission inventories proportionally affect CAMx outputs; these biases are systematically corrected using the RF model, as presented in Fig. 3b and discussed in the Results and discussion section.

3. Results and discussion

3.1. CAMx predictions

Fig. 1 displays the CAMx-simulated mean Cu concentrations across Europe, averaged over the period from 2010 to 2019. The spatial distribution reveals high concentrations in urban areas and cities, with lower levels in sparsely populated and rural regions. Notably, elevated concentrations are present in Southern England, the Benelux region, and the Po Valley, which align with the NO_x distribution patterns, typically driven by vehicular emissions (Ciarelli et al., 2021; Duncan et al., 2016; Schaap et al., 2013). In Fig. 1 observational data is overlaid, showing coverage across most of Western and Central Europe, with significant gaps in Eastern Europe and the Balkans, emphasizing the necessity for additional monitoring initiatives in Eastern Europe. The initial comparisons indicate that CAMx exhibits an average negative bias of a factor of around 7 when compared to observations.

Fig. 2 shows a density scatter plot comparing CAMx predictions with observations. This illustrates that the CAMx bias varies across the concentration range, from an average underestimation of less than a factor of 2 at lower concentrations to an underestimation of more than a factor of 10 at higher concentrations. This results in a moderate Pearson correlation coefficient of r = 0.43. As mentioned in Section 2.3, this underestimation may result from several factors: (1) uncertainties in the brake wear emission inventory; (2) the coarse resolution of CAMx, which limits its ability to capture highly localized concentrations; (3) unaccounted sources of Cu, such as industrial emissions, railways, and resuspended particles; and (4) uncertainties in meteorological inputs

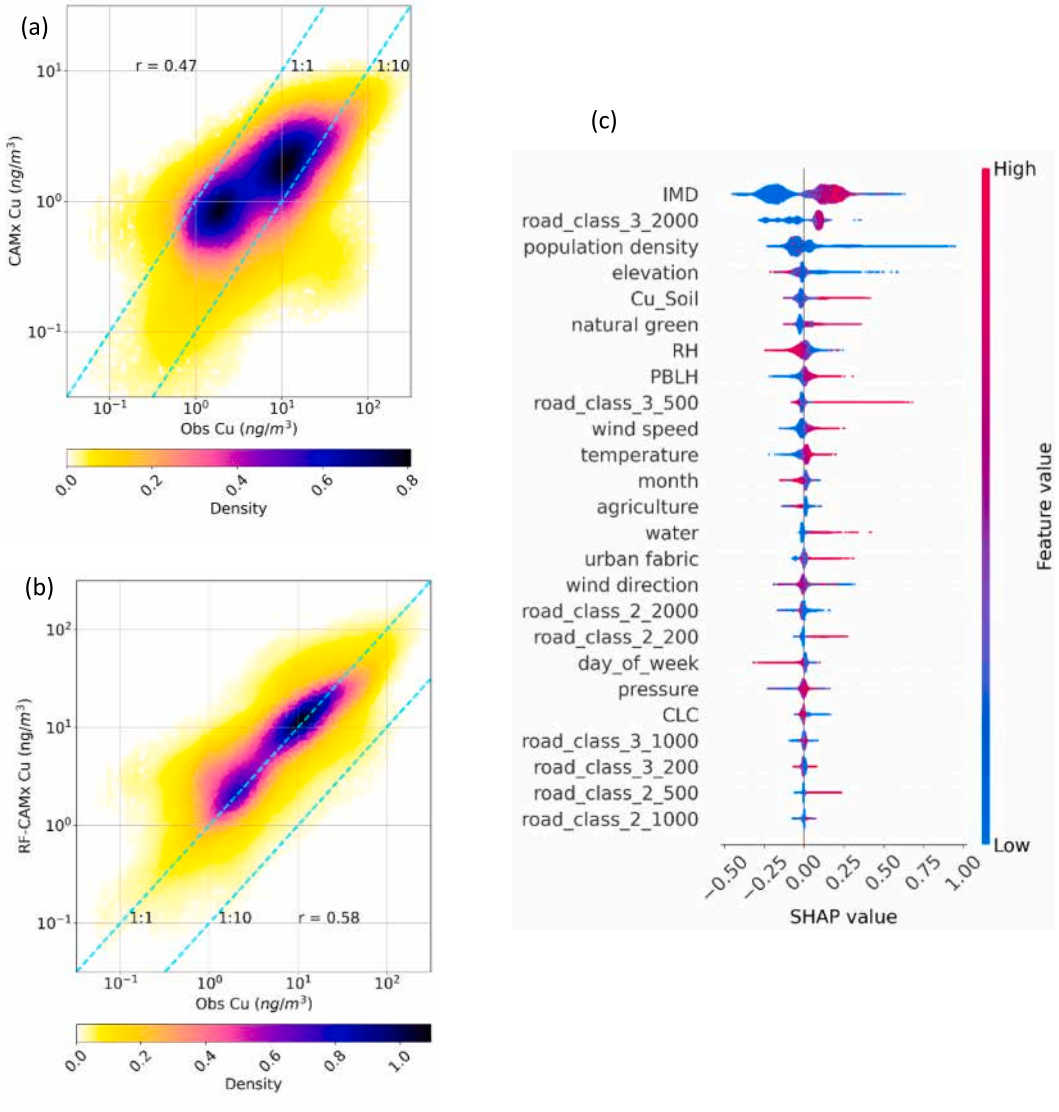

Fig. 2. (a) Scatter plot between CAMx simulated Cu (ng/m^3) and observed Cu concentration (ng/m^3) from 152 locations over Europe (b) Scatter plot between RF-CAMx predicted Cu and observed Cu concentrations (ng/m^3), where color represents data density. (c) SHAP value analysis of feature importance in the RF model for Cu predictions, highlighting the 25 most important features. Each point represents a SHAP value, which quantifies the contribution of a specific feature to an individual prediction. A higher absolute SHAP value indicates a stronger influence on the model's output. The color gradient represents the feature magnitude, with higher values shown in red and lower values in blue. Features with a wider spread of SHAP values exhibit greater variability in their influence. (For interpretation of the references to color in this figure legend, the reader is referred to the web version of this article.)

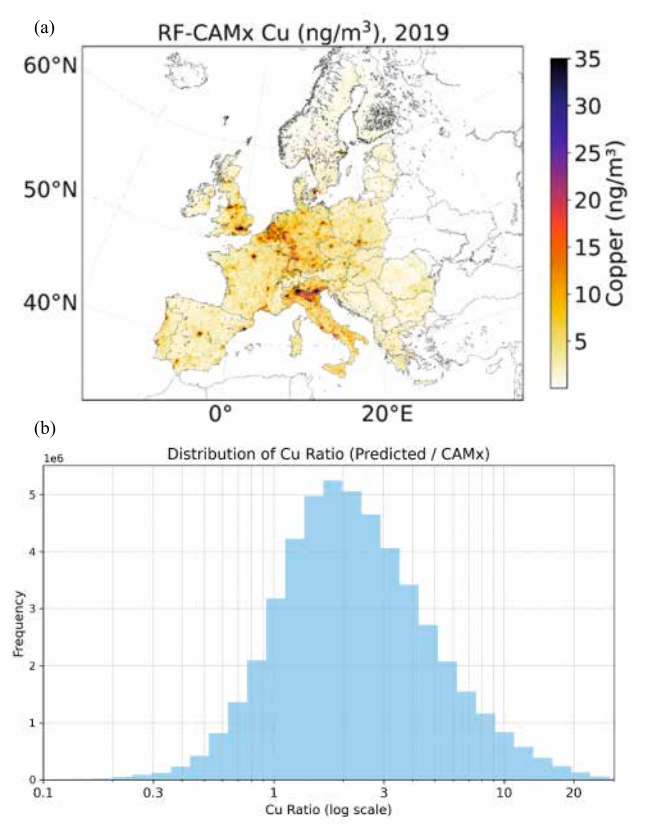

Fig. 3. (a) Annual mean surface Cu concentration over Europe for the year 2019 at spatial resolution of 0.0025° × 0.005° (~250 m) from RF-CAMx model, (b) Histogram showing distribution of ratio of RF-CAMx Cu and CAMx Cu over Europe for year 2019.

from the WRF model, which together with CAMx parameterization schemes can introduce errors in simulating the transport, dispersion, and deposition of Cu. The spatial variation in CAMx bias, suggests that CAMx outputs or emission inventories cannot be accurately corrected with a single scaler. The bias magnitude correlates with local features, such as urban fraction, IMD, and road variables, while showing low correlations with other anthropogenic emission indicators, confirming that traffic emissions remain the most important source of Cu in most of Europe. To address this, we have incorporated land-use variables into a random forest framework to correct CAMx biases, accounting for the fine-scale variability of these emission indicators.

3.2. RF model performance

We validated the RF model following different approaches. First, we followed the conventional validation approach, utilizing 80 % of the total dataset for training and 20 % for validation (Grange et al., 2018; Wu et al., 2023), which resulted in a high Pearson's correlation of 0.75 (Fig. S3(a)). In another approach, we validated the trained model on locations not included in the training by setting aside about 10 % of the monitoring stations each time, ensuring that all stations were eventually treated as unseen. This was done to ensure the spatial robustness of the model. Fig. 2(b) illustrates a density scatter plot comparing RF-CAMx predicted Cu for unseen sites with observed values, demonstrating an increase in Pearson's correlation coefficient from 0.43 with CAMx to 0.58 with RF-CAMx. In contrast to the CAMx validation results (Fig. 2 (a)), the RF predictions align closely with the 1:1 line across all concentrations, indicating that the prediction is consistent across all concentration ranges. We utilized the resulting model to make daily Cu predictions over the period of 2010–2019. We also conducted a leave-one-year-out validation process by excluding one year for validation purposes and trained the model with the remaining dataset. This resulted in a Pearson's correlation coefficient of 0.69 (Fig. S3(b)), which highlights the model's ability to effectively predict multiyear Cu concentrations. In the leave-one-year-out validation, the model demonstrates a mean Pearson's r of 0.71 with a standard deviation of 0.09, and a mean RMSE of 18.2 ng/m^3 with a standard deviation of 4.9 ng/m^3, this small variation indicates the model's robust and consistent temporal performance (Fig. S4). Fig. S7(a) compares the performance of the RF model presented here (RF-CAMx) with the RF model that is not anchored to CAMx (RF). The non-anchored model demonstrated a good Pearson's correlation of 0.61 and a low root mean squared error (RMSE) of 20.22 ng/m^3 in the validation phase. However, it globally shows over-predictions and inconsistencies across all concentration ranges (Fig. S7 (b)), which shows that anchoring the model to CAMx enhances robustness, as it retains the physical model's broader spatial structures while correcting for local biases. A list of detailed validation matrices is given in Table S3 for all used RF based models and validation methodologies.

3.3. Importance of predictor variables

The relative importance of each predictor in the RF was identified through feature importance and SHapley Additive exPlanations (SHAP) analysis (Figs. 2(c) and S5). Both methods highlight that impervious surface density (IMD), population density, road class 3, Cu concentrations in topsoil (see Table S1), and PBLH, significantly influence predictions. SHAP values illustrate how each input variable contributes to individual predictions (Lundberg and Lee, 2017), and the corresponding plot shown in Fig. 2(c) reports the top 25 most influential variables. Among these, IMD, road class 3 within a 2000 m buffer, and population density are the three most critical features. Higher IMD which corresponds to more buildup values is associated with bigger predicted log ratio of observed and CAMx Cu which corresponds to higher predicted Cu concentrations. Similarly, a higher density of road class 3 positively impacts predictions, while a lower density for the same negatively affects copper concentrations. This supports that Cu is primarily associated with vehicular non-exhaust emissions, as areas with extensive roads and concrete surfaces typically experience elevated Cu concentrations. Conversely, elevation shows an inverse relationship, with lower elevations associated with higher Cu concentrations. Population density appears to act as a balancing factor, potentially correcting any overestimations of Cu concentrations driven by IMD or road networks. The positive impact of population density at lower values indicates that pollution sources in these areas are influenced more by infrastructure or localized factors rather than by population density alone.

3.4. Spatial distributions of Cu over Europe

We predicted spatially downscaled and corrected maps of daily mean atmospheric Cu concentration over Europe for a 10-years period (2010–2019) using the trained RF model. The predicted Cu maps are at a fine spatial resolution of 0.0025° × 0.005° (~250 m) over Europe, and the annual mean for the year 2019 is shown in Fig. 3(a). The predicted Cu map of each day consists of approximately 70 million grid data points for Cu over the land area of Europe (excluding the ocean), which amounts to 250 billion prediction points over 10 years which makes it computationally expensive. The spatial distribution of Cu concentrations from RF-CAMx closely resembles that from the CAMx simulation across Europe but with significantly higher concentration levels at most of the locations. Figs. 3(b) and S6 show the ratio between Random Forest–corrected CAMx (RF-CAMx) and the original CAMx predictions, presented as a probability density function and a spatial map, respectively. The ratio centers around 2, indicating that CAMx underestimates Cu concentrations mostly a factor of two. This underestimation is likely influenced by uncertainties in emission inventories, especially for brake wear, where emission factors vary with driving conditions and are hard

to quantify. While this level of bias is reasonable given these uncertainties, the wide range in ratios from <1 to >10 highlights substantial spatial variability. Higher correction factors are seen in urban and roadside areas, while rural regions require less adjustment, supporting the initial assumption that Cu is largely traffic-related. This spatial spread also reflects a key limitation of coarse-resolution chemical transport models like CAMx, which cannot resolve fine-scale heterogeneity in emissions. The Random Forest model overcomes this by using high-resolution land use data to both downscale and bias-correct CAMx outputs. Fig. 4 presents the annual mean Cu concentrations from both the CAMx and RF-CAMx models for two regional domains: one around central Europe (4 to 14°E, 43 to 48°N) and another around the Benelux region (−2 to 10°E, 48 to 53°N). Both models are comparable in identifying the spatial distributions and hotspots. However, the RF model resolves local spatial features more effectively due to its finer resolution. We observe comparatively lower Cu concentrations in the eastern part of Europe, which is typically a hotspot for organic pollutants. During the modelling process, we have limited the number of ground based Cu observations from the eastern region. We expect that incorporating more data from this region in future analyses will result in further improvements in the model's performance for sites in the eastern region.

The results in Figs. 3 and 4 illustrate spatial distributions of Cu at both the European and regional scales. It shows that Po Valley, Northwestern Europe (including the Benelux region and western Germany), and major cities such as London, Paris, and Madrid are the key hotspots for Cu. Cu levels are generally higher in urban areas, with rural regions exhibiting lower concentrations. Notably, elevated Cu concentrations are observed in proximity to road networks, particularly in areas connecting major cities. For example, the elevated concentrations are observed along the major road from Lyon to Marseille and the transport network between Milan and Rimini through Bologna in Italy, as well as the road network linking Warsaw to Bydgoszcz and the Gdańsk coast in Poland, are particularly notable. The Po Valley is a significant hotspot where both background and urban Cu concentrations are elevated. The region is characterized by a valley-like geography that limits atmospheric ventilation, combined with substantial emission sources, leading to a widespread distribution of Cu. These conditions make the RF-CAMx model particularly relevant for accurately representing concentration distribution in this region. The high-resolution map in the Benelux region further demonstrates that Cu concentrations closely follow road networks and correlate with urban density.

To explore the distribution at the local scale, we analyzed Cu concentrations, focusing on major cities such as Paris, Brussels, London, and Warsaw. The results are presented in Fig. 5(a–d), which covers a 1° × 1° area to include the urban landscape and surrounding regions. Fig. 5(a–d) reveals significant fluctuations in Cu concentrations within these cities, with concentrations tending to be highest in built-up areas and along major roads. Fig. 5(e) illustrates Cu concentrations in a 0.12° × 0.12° area for ten European cities (Milan, Paris, Warsaw, Ljubljana, Bern, Madrid, Berlin, Rome, Brussels, and London). Here, the selected area for each city is slightly smaller than one CAMx grid cell. The analysis is based on yearly average concentrations. The plot shows mean, median, and interquartile range (IQR) of annual mean Cu within the selected city domain to describe Cu distribution. Notably, the mean Cu concentration is often higher than the median, indicating a right-skewed distribution due to a few elevated concentration values. The IQR reveals a considerable variability around the median in most cities, sometimes exceeding half the mean concentration. Among the cities, London, Madrid, and Paris have higher concentrations and IQRs, while Warsaw, Ljubljana, and Bern have lower levels. Within high-concentration cities, differences are evident: for instance, London has a median Cu concentration that is 7 ng/m^3 higher than Milan's, while the mean concentration is 14 ng/m^3 greater. This indicates that London has a larger number of high-concentration areas. Madrid has a higher IQR than Milan but lower mean and median concentrations. Overall, the distribution of median concentrations across cities demonstrates that intra-cities variations are equally important as those between cities as shown in the last box and whisker plot of the Fig. 5(e).

3.5. Temporal trends in Cu

We used high-resolution daily mean Cu concentrations to project trends on weekly, monthly, and annual scales for the ten selected cities. The mean Cu concentration shows a 25 % decrease on Saturdays and a 37 % decrease on Sundays (Fig. 6a). This decline occurs due to reduced traffic levels during the weekend, leading to lower Cu levels (Mues et al., 2014). Similar weekly cycles have been observed for CO and NOx at urban and traffic sites across Europe (Masiol et al., 2017).

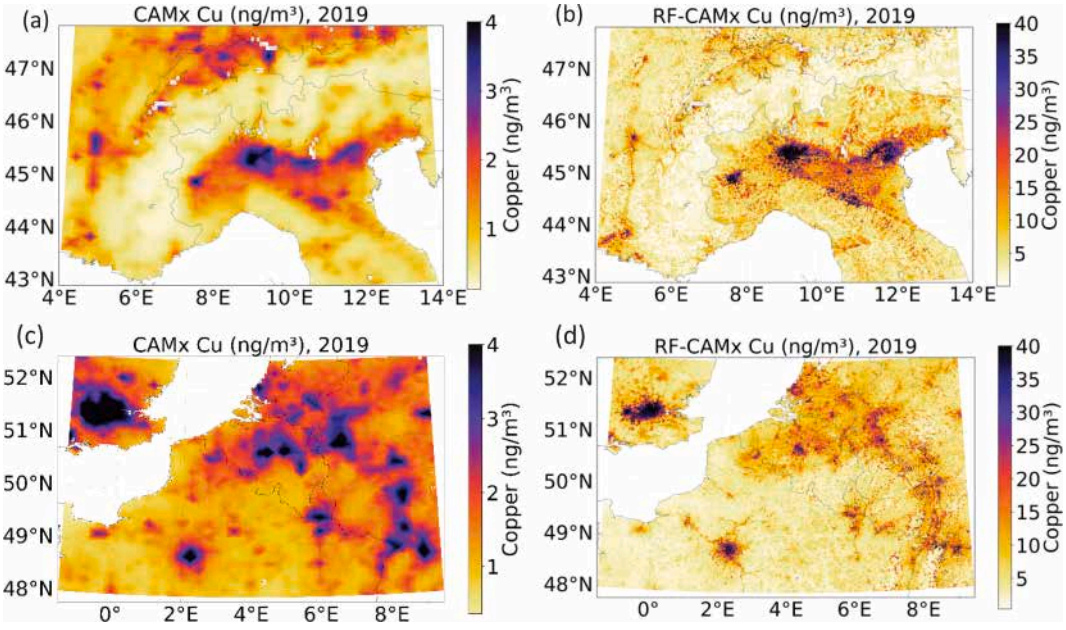

Fig. 4. (a) Coarse resolution from CAMx and (b) downscaled Cu from RF-CAMx over central Europe including Po valley and south Europe, Switzerland, eastern France, etc. (c) Coarse resolution from CAMx and (d) downscaled Cu from RF-CAMx part of northwest Europe Benelux region and west Europe.

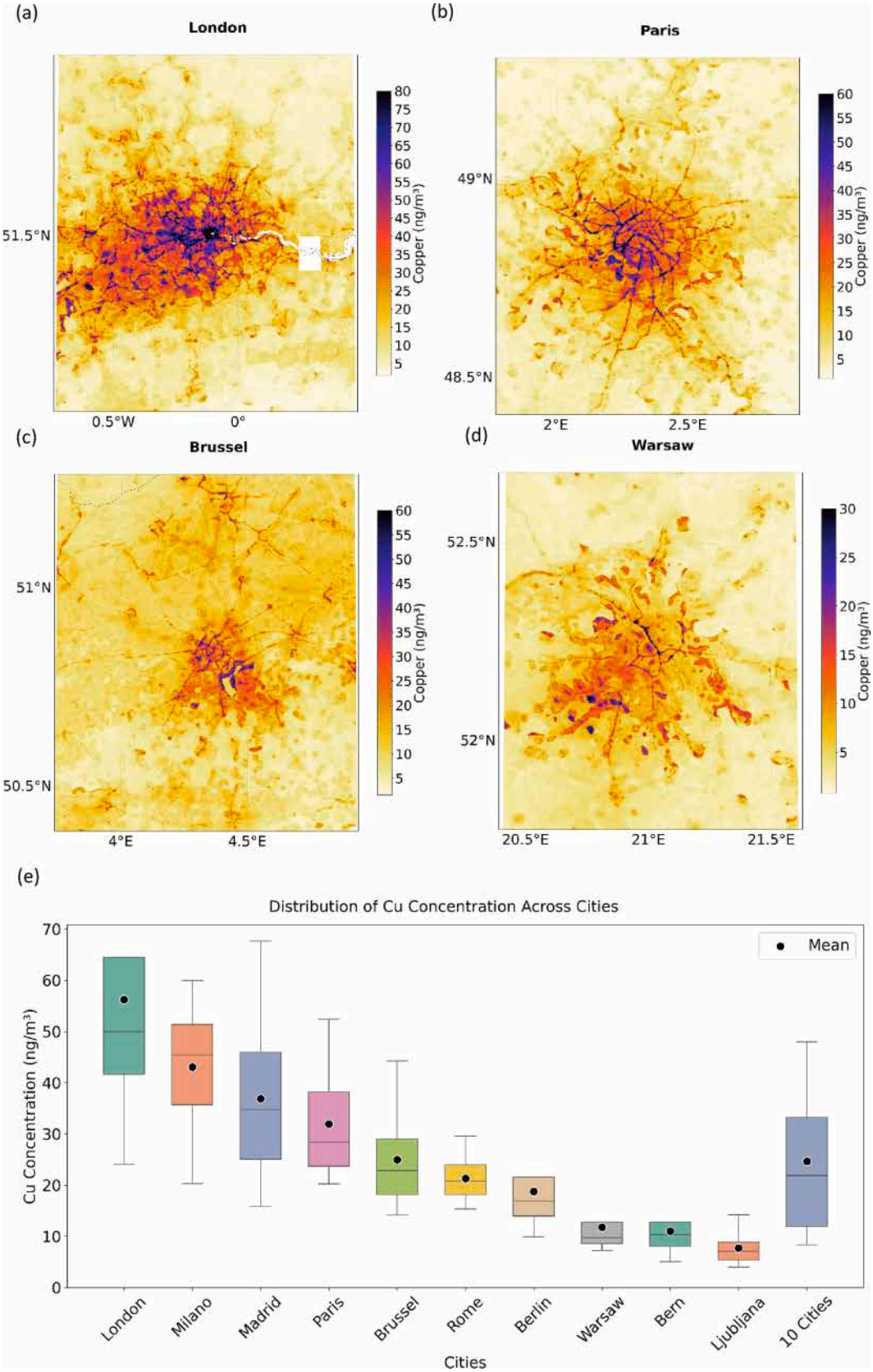

Fig. 5. Fine-scale map zoomed to local scale, capturing local distribution of Cu for cities (a) London, (b) Paris, (c) Brussel and (d) Warsaw, here blank area shows masking of waterbodies, (e) Spatial distribution of Cu concentration in 0.12° × 0.12° degree domain around the center of the city. Here the box represents the 25 %–75 % interquartile range (IQR), the line inside indicates the median, and the black dots represent the mean for each city. Whiskers extend to 1.5 times the IQR beyond the first and third quartiles. For some cities, whiskers are not visible because the most extreme non-outlier values are very close to the quartiles, and all more distant values lie outside the whisker range.

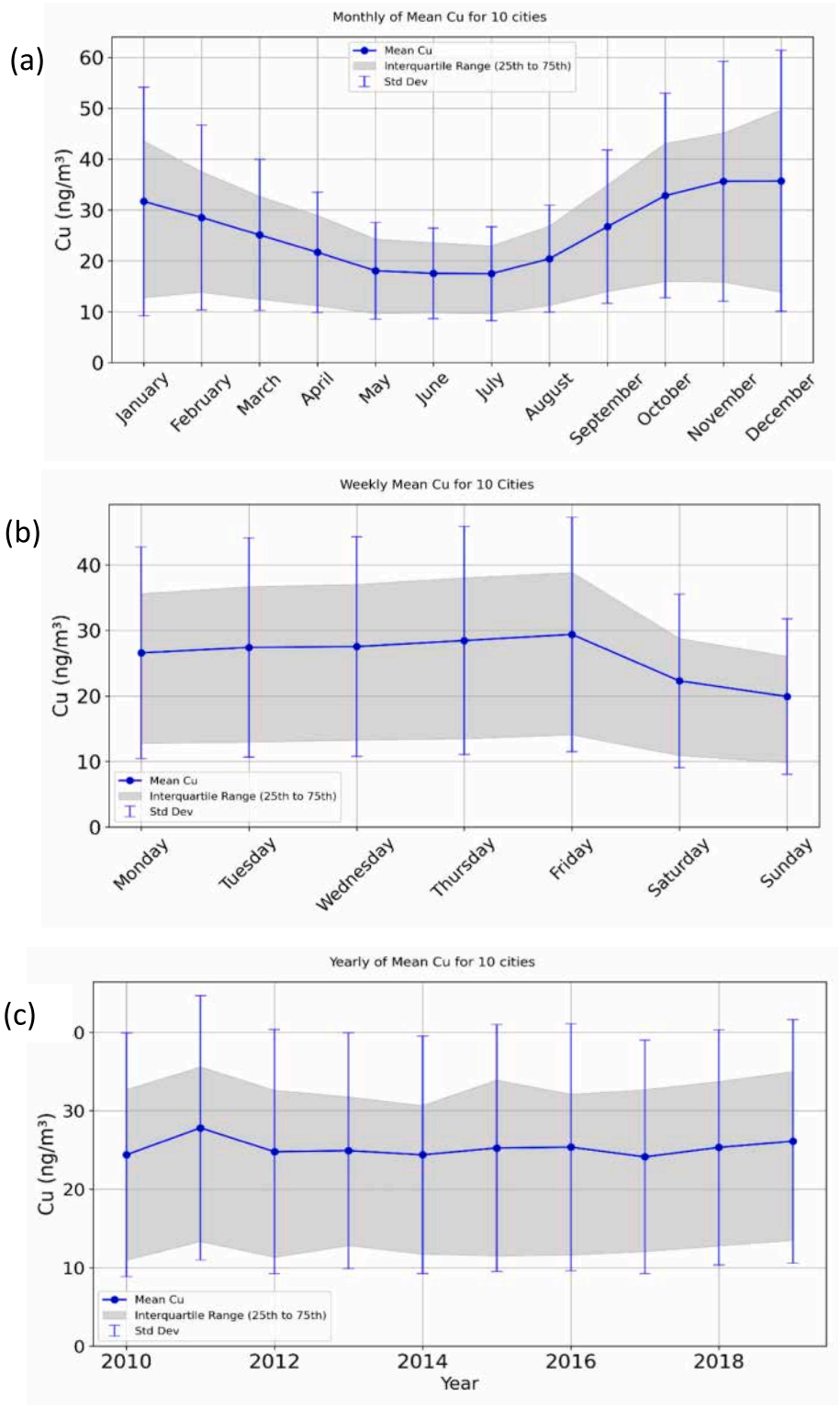

Fig. 6. Temporal trend of atmospheric Cu showing (a) Weekly cycle, (b) Monthly cycle, and (c) Annual trend in Cu concentration for the European 10 cities selected in Fig. 5(e).

The monthly averages indicate that there are higher Cu concentrations during the winter months, with a 30 % decrease observed in the summer (Fig. 6b). This variation is primarily driven by seasonal changes in meteorological conditions. Winter months typically feature stable weather and lower PBLH, which favor pollutant accumulation, while summer conditions are more unstable, promoting transport and dispersion. Similar seasonal patterns have been observed for CO, NO, NO_2, NOx, PM_{10}, and $PM_{2.5}$ concentration in the Po Valley (Bigi et al., 2012; Masiol et al., 2017) and for CO and NOx across Europe (Lacima et al., 2023). However, a similar monthly cycle is not consistently observed in regions with weaker meteorological patterns, such as the Mediterranean. As shown in Fig. S9, the monthly Cu concentration trend is inconsistent in 7 out of 12 Mediterranean cities, where the influence of the meteorological cycle is less pronounced compared to other parts of

Europe.

The annual variation in Cu concentrations shows no significant increasing or decreasing trend when averaged across the ten cities (Fig. 6c). However, distinct trends can be seen in individual cities (Fig. S3b). Brussels, Warsaw, Ljubljana, London, and Paris have experienced an increase in concentration trends, while Milan and Rome show decreasing concentrations. By contrast, Bern, Madrid, and Berlin exhibit no significant trends. Overall, while exhaust emissions of PM and NOx have fallen by 50 % and 40 %, respectively, over the past two decades (2000–2018) across Europe, brake wear emissions have remained largely unchanged (Denier van der Gon et al., 2018; Monforti Ferrario et al., 2022).

3.6. Population exposure to Cu

Our results indicate that Cu concentrations are higher in densely populated areas, with half of the population exposed to levels exceeding 8 ng/m^3. Approximately 12 million persons are exposed to Cu concentrations greater than 40 ng/m^3 (see Figs. 7(a) and S10), while 56 million individuals across Europe are exposed to more than 20 ng/m^3 of Cu. The population-weighted concentrations (methodology in Section S1.1) by country shown in Fig. 7(b) indicate that Italy, Belgium, the Netherlands, and the United Kingdom experience higher average exposures than other countries.

Currently, no standard limit for Cu has been set by environmental regulatory agencies. However, based on studies of brake-wear PM_{10} chemical composition, Cu concentration of 40 ng/m^3 corresponds to about 900 ng/m^3 of PM_{10} brake wear which contains approximately 800 ng/m^3 of Fe (~90 %) (Daellenbach et al., 2020). Fe is also reported to exert high oxidative stress through reactive oxygen species (ROS) and deteriorate pulmonary response (Galli et al., 2024). For context, the World Health Organization's proposed guidelines for PM_{10} are set at an annual average of 15 μg/m^3. This highlights that brake wear emissions continue to be a significant source of PM_{10} and particularly of redox-active metals, especially in urban areas, able to induce oxidative stress.

4. Conclusions

The CAMx modeling coupled with TNO's non-exhaust emission inventory for Cu largely captured the spatial distribution of vehicular non-exhaust Cu, emphasizing urban areas as pollution hotspots across Europe. The integrated CAMx-RF model maps the non-linear relationships with site-specific factors such as land use, road networks, population density, and topsoil Cu, thereby enhancing prediction accuracy compared to CAMx and enabling high-resolution downscaling to approximately 250 m. This integrated approach is expected to accurately model other pollutants using chemical transport model simulations with suitable land-use proxies.

High-resolution daily predictions offer a detailed understanding of the spatial and temporal trends of Cu. The distribution pattern identifies cities, urban environments, and areas along road networks as the primary Cu hotspots, in line with anticipated patterns for vehicle-derived particulate matter. This finding emphasizes the need for focused attention on this toxic, unregulated pollutant from a public health standpoint in the identified hotspot regions. The temporal trends of Cu levels, such as those observed on a monthly basis, are largely driven by meteorological cycles. In contrast, the weekly and annual trends are primarily driven by emission variations. These daily predictions provide invaluable insight into the impact of emissions and meteorology on Cu distribution, which is crucial for effective air quality management and long-term planning at both urban and regional levels. These distribution trends allow agencies to assess the effectiveness of their plans, verify policies, and identify periods of high pollution for issuing health advisories. The introduction of the EURO 7 regulations includes limits on non-exhaust emissions, such as PM_{10} from brake wear in light-duty vehicles (LDVs). The modelling approach used in this study, when applied with revised emission estimates based on EURO 7 will be crucial in assessing the spatial effectiveness of these regulations on non-exhaust emissions.

The high-resolution daily Cu maps produced by this approach provide valuable insights at regional, national, and local scales particularly useful for epidemiological studies on the chronic and acute health effects of brake wear PM composition. The heterogeneous distribution of Cu at a fine resolution at the local scales underscores the need for more precise measurement campaigns to account for intra-city variations. It also highlights the need to place greater emphasis on mobile measurements to gain a deeper understanding of the spatial distribution of non-exhaust pollution. Furthermore, there is a need for additional measurements in Eastern Europe, where data is relatively sparse.

Aerosols from non-exhaust sources consist of various particles like Zn, Fe, and Sb, while Cu is also emitted by other sources like railways, industries, and dust resuspension which should also be further investigated. Therefore, additional studies focusing on the detailed and comprehensive source apportionment of urban aerosols remain essential. This will notably enable the inclusion of additional non-exhaust tracers in the modeling, thus accounting for the accurate share of Cu from non-exhaust that potentially leads to reduced uncertainties in predictions. To improve predictions, enhance health impact assessment, and support regulatory purposes, a continuous improvement in the emission inventory for non-exhaust sources is required, including better accounting of sources such as EVs and the development of emission inventories for heavy metals. Overall, this study provides valuable insights for regulating vehicle emissions, public issuing health advisories on toxic pollutants, gathering exposure data for epidemiological studies, and providing information for both short- and long-term air pollution mitigation planning.

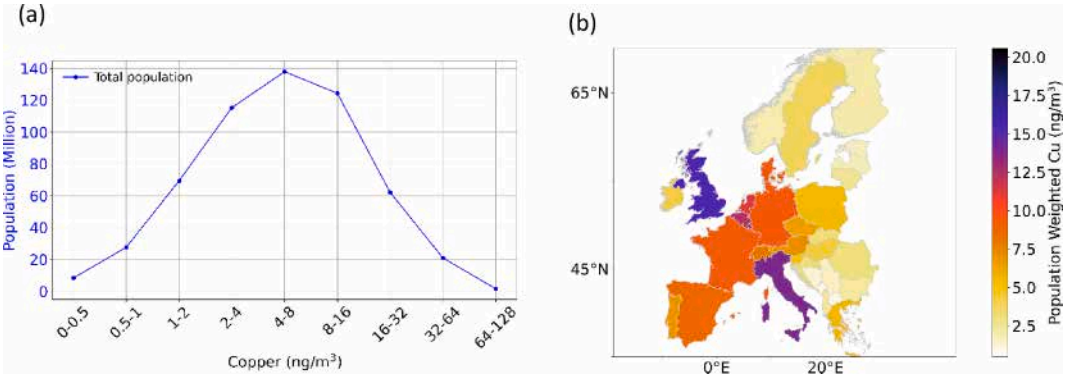

Fig. 7. (a) Total exposed population to the given bin of Cu concentration over Europe, (b) Population weighted Cu concentration for each country over Europe.

CRediT authorship contribution statement

Abhishek Upadhyay: Writing – original draft, Visualization, Validation, Software, Methodology, Formal analysis, Data curation, Conceptualization. **Jianhui Jiang:** Writing – review & editing, Software, Data curation. **Yun Cheng:** Writing – review & editing, Software, Data curation. **Petros Vasilakos:** Writing – review & editing, Software, Data curation. **Ying Chen:** Writing – review & editing, Software, Methodology. **Daniel Trejo Banos:** Writing – review & editing, Software, Methodology, Data curation. **Benjamin Flückiger:** Writing – review & editing, Software, Resources, Methodology. **Manousos I. Manousakas:** Writing – review & editing, Data curation. **André S.H. Prévôt:** Writing – review & editing, Funding acquisition, Data curation. **Robin L. Modini:** Writing – review & editing, Conceptualization. **Ana Sánchez de la Campa:** Writing – review & editing, Data curation. **Andrea Schemmel:** Writing – review & editing, Data curation. **Andrés Alastuey:** Writing – review & editing, Data curation. **Benjamin Bergmans:** Writing – review & editing, Data curation. **Célia A. Alves:** Writing – review & editing, Data curation. **Christoph Hueglin:** Writing – review & editing, Data curation. **Cristina Colombi:** Writing – review & editing, Data curation. **Cristina Reche:** Writing – review & editing, Data curation. **Daniel Sánchez-Rodas:** Writing – review & editing, Data curation. **Dario Massabò:** Writing – review & editing, Data curation. **Evangelia Diapouli:** Writing – review & editing, Data curation. **Federico Mazzei:** Writing – review & editing, Data curation. **Franco Lucarelli:** Writing – review & editing, Data curation. **Gaëlle Uzu:** Writing – review & editing, Data curation. **Imre Salma:** Writing – review & editing, Data curation. **Jean-Luc Jaffrezo:** Writing – review & editing, Funding acquisition, Data curation. **Jesús D. de la Rosa:** Writing – review & editing, Data curation. **Jolanda E. Reusser:** Writing – review & editing, Data curation. **Kostas Eleftheriadis:** Writing – review & editing, Data curation. **Laurent Y. Alleman:** Writing – review & editing, Data curation. **Mark Scerri:** Writing – review & editing, Data curation. **Mirko Severi:** Writing – review & editing, Data curation. **Olivier Favez:** Writing – review & editing, Data curation. **Paolo Prati:** Writing – review & editing, Data curation. **Rita Traversi:** Writing – review & editing, Data curation. **Roberta Vecchi:** Writing – review & editing, Data curation. **Silvia Becagli:** Writing – review & editing, Data curation. **Silvia Nava:** Writing – review & editing, Data curation. **Sonia Castillo:** Writing – review & editing, Data curation. **Sophie Darfeuil:** Writing – review & editing, Data curation. **Stuart K. Grange:** Writing – review & editing, Data curation. **Xavier Querol:** Writing – review & editing, Funding acquisition, Data curation. **Zsófia Kertész:** Writing – review & editing, Data curation. **Giancarlo Ciarelli:** Writing – review & editing, Conceptualization. **Nicole Probst-Hensch:** Writing – review & editing, Funding acquisition. **Danielle Vienneau:** Writing – review & editing, Investigation. **Jeroen Kuenen:** Writing – review & editing, Investigation, Data curation. **Hugo Denier Van Der Gon:** Writing – review & editing, Investigation, Data curation. **Kaspar R. Daellenbach:** Writing – review & editing, Supervision, Funding acquisition, Data curation. **Ekaterina Krymova:** Writing – review & editing, Software, Project administration, Methodology, Conceptualization. **Kees de Hoogh:** Writing – review & editing, Data curation. **Imad El-Haddad:** Writing – original draft, Supervision, Resources, Project administration, Methodology, Funding acquisition, Conceptualization.

Declaration of competing interest

The authors declare that they have no known competing financial interests or personal relationships that could have appeared to influence the work reported in this paper.

Acknowledgements

This work acknowledges the following contributions, without which it would not have been feasible: PSI team acknowledge funding from Swiss data science centre (grant AURORA), the Swiss federal office of environment (FOEN) and the European Union's Horizon 2020 research and innovation programme under the Marie Skłodowska-Curie grant agreement No 884104 (PSI-FELLOW-III-3i). This project is partially funded by the Swiss Data Science Center (SDSC) collaborative projects grant (C20-08). For French sites, personnel from regional air quality monitoring networks – namely Atmo Haut-de-France, Atmo Normandie, Atmo Grand-Est, Atmo Nouvelle-Aquitaine, Atmo Auvergne Rhône-Alpes and Atmo Sud – as well as S. Conil (ANDRA) are warmly acknowledged for filter and data collection. A large part of the trace element analyses of these samples was performed on the analytical plateform Air O Sol at IGE. JJ acknowledges the National Natural Science Foundation of China (42207122), and the National Key Research and Development Program of China (2023YFC3710400). University of Aveiro team acknowledge the support to CESAM by FCT/MCTES (UIDP/50017/2020+UIDB/50017/2020+LA/P/0094/2020). Regarding Italian sites, regional projects and collaborations – PATOS (Particolato Atmosferico in Toscana), funded by Tuscany Region and KALOS funded by Calenzano (Florence) municipality are warmly acknowledged. The Hungarian Research, Development and Innovation Office (contract: Advanced 150835) funded the experimental work in Hungary. This work also acknowledges RI-URBANS and EBAS database and all measurement projects for Cu observation, ECCAD tool for emission analysis.

Appendix A. Supplementary data

Supplementary data to this article can be found online at https://doi.org/10.1016/j.envint.2025.109615.

Data availability

Data used in the manuscript figures are available at link. Model data can be available on request from corresponding authors. Observed Cu concentration will be available on request from station specific measurement group.

References

Alves, D.D., Riegel, R.P., Klauck, C.R., Ceratti, A.M., Hansen, J., Cansi, L.M., Pozza, S.A., de Quevedo, D.M., Osório, D.M.M., 2020. Source apportionment of metallic elements in urban atmospheric particulate matter and assessment of its water-soluble fraction toxicity. Environ. Sci. Pollut. Res. 27, 12202–12214. https://doi.org/10.1007/s11356-020-07791-8.

Beelen, R., Hoek, G., Raaschou-Nielsen, O., Stafoggia, M., Andersen, Z.J., Weinmayr, G., Hoffmann, B., Wolf, K., Samoli, E., Fischer, P.H., Nieuwenhuijsen, M.J., Xun, W.W., Katsouyanni, K., Dimakopoulou, K., Marcon, A., Vartiainen, E., Lanki, T., Yli-Tuomi, T., Oftedal, B., Schwarze, P.E., Nafstad, P., Faire, U.D., Pedersen, N.L., Östenson, C.-G., Fratiglioni, L., Penell, J., Korek, M., Pershagen, G., Eriksen, K.T., Overvad, K., Sørensen, M., Eeftens, M., Peeters, P.H., Meliefste, K., Wang, M., Bueno-de-Mesquita, H.B., Sugiri, D., Krämer, U., Heinrich, J., de Hoogh, K., Key, T., Peters, A., Hampel, R., Concin, H., Nagel, G., Jaensch, A., Ineichen, A., Tsai, M.-Y., Schaffner, E., Probst-Hensch, N.M., Schindler, C., Ragettli, M.S., Vilier, A., Clavel-Chapelon, F., Declercq, C., Ricceri, F., Sacerdote, C., Galassi, C., Migliore, E., Ranzi, A., Cesaroni, G., Badaloni, C., Forastiere, F., Katsoulis, M., Trichopoulou, A., Keuken, M., Jedynska, A., Kooter, I.M., Kukkonen, J., Sokhi, R.S., Vineis, P., Brunekreef, B., 2015. Natural-cause mortality and long-term exposure to particle components: an analysis of 19 European cohorts within the multi-center ESCAPE Project. Environ. Health Perspect. 123, 525–533. https://doi.org/10.1289/ehp.1408095.

Bertrand, J.-M., Meleux, F., Ung, A., Descombes, G., Colette, A., 2023. Technical note: improving the European air quality forecast of the Copernicus atmosphere monitoring service using machine learning techniques. Atmos. Chem. Phys. 23, 5317–5333. https://doi.org/10.5194/acp-23-5317-2023.

Bigi, A., Ghermandi, G., Harrison, R.M., 2012. Analysis of the air pollution climate at a background site in the Po valley. J. Environ. Monit. 14, 552–563. https://doi.org/10.1039/C1EM10728C.

Birmili, W., Allen, A.G., Bary, F., Harrison, R.M., 2006. Trace metal concentrations and water solubility in size-fractionated atmospheric particles and influence of road traffic. Environ. Sci. Technol. 40, 1144–1153. https://doi.org/10.1021/es0486925.

Breiman, L., 2001. Random forests. Mach. Learn. 45, 5–32. https://doi.org/10.1023/A:1010933404324.

Charron, A., Polo-Rehn, L., Besombes, J.-L., Golly, B., Buisson, C., Chanut, H., Marchand, N., Guillaud, G., Jaffrezo, J.-L., 2019. Identification and quantification of

particulate tracers of exhaust and non-exhaust vehicle emissions. Atmos. Chem. Phys. 19, 5187–5207. https://doi.org/10.5194/acp-19-5187-2019.
Chelhaoui, Y., El Ass, K., Lachatre, M., Bouakline, O., Khomsi, K., El Moussaoui, T., Arrad, M., Eddaif, A., Albergel, A., 2024. A new optimized hybrid approach combining machine learning with WRF-CHIMERE model for PM10 concentration prediction. Model. Earth Syst. Environ. 10, 5687–5701. https://doi.org/10.1007/s40808-024-02086-0.
Chen, Z.-Y., Zhang, R., Zhang, T.-H., Ou, C.-Q., Guo, Y., 2019. A kriging-calibrated machine learning method for estimating daily ground-level NO2 in mainland China. Sci. Total Environ. 690, 556–564. https://doi.org/10.1016/j.scitotenv.2019.06.349.
Chen, J., Hoogh, K. De, Gulliver, J., Ho, B., Hertel, O., Ketzel, M., Bauwelinck, M., Donkelaar, A. Van, Hvidtfeldt, U.A., Katsouyanni, K., Janssen, N.A.H., Martin, R.V, Samoli, E., Schwartz, P.E., Stafoggia, M., Bellander, T., Strak, M., Wolf, K., Vienneau, D., Vermeulen, R., Brunekreef, B., Hoek, G., 2019. A comparison of linear regression, regularization, and machine learning algorithms to develop Europe-wide spatial models of fi ne particles and nitrogen dioxide, 130. https://doi.org/10.1016/j.envint.2019.104934.
Chen, J., Rodopoulou, S., de Hoogh, K., Strak, M., Andersen, Z.J., Atkinson, R., Bauwelinck, M., Bellander, T., Brandt, J., Cesaroni, G., Concin, H., Fecht, D., Forastiere, F., Gulliver, J., Hertel, O., Hoffmann, B., Hvidtfeldt, U.A., Janssen, N.A.H., Jöckel, K.-H., Jørgensen, J., Katsouyanni, K., Ketzel, M., Klompmaker, J.O., Lager, A., Leander, K., Liu, S., Ljungman, P., MacDonald, C.J., Magnusson, P.K.E., Mehta, A., Nagel, G., Oftedal, B., Pershagen, G., Peters, A., Raaschou-Nielsen, O., Renzi, M., Rizzuto, D., Samoli, E., van der Schouw, Y.T., Schramm, S., Schwarze, P., Sigsgaard, T., Sørensen, M., Stafoggia, M., Tjønneland, A., Vienneau, D., Weinmayr, G., Wolf, K., Brunekreef, B., Hoek, G., 2021. Long-term exposure to fine particle elemental components and natural and cause-specific mortality—a pooled analysis of eight European cohorts within the ELAPSE project. Environ. Health Perspect. 129, 47009. https://doi.org/10.1289/EHP8368.
Chiari, M., Yubero, E., Calzolai, G., Lucarelli, F., Crespo, J., Galindo, N., Nicolás, J.F., Giannoni, M., Nava, S., 2018. Comparison of PIXE and XRF analysis of airborne particulate matter samples collected on Teflon and quartz fibre filters. Nucl. Instrum. Methods Phys. Res. Sect. B 417, 128–132. https://doi.org/10.1016/j.nimb.2017.07.031.
Ciarelli, G., Jiang, J., El Haddad, I., Bigi, A., Aksoyoglu, S., Prévôt, A.S.H., Marinoni, A., Shen, J., Yan, C., Bianchi, F., 2021. Modeling the effect of reduced traffic due to COVID-19 measures on air quality using a chemical transport model: impacts on the Po Valley and the Swiss Plateau regions. Environ. Sci.: Atmos. 1, 228–240. https://doi.org/10.1039/D1EA00036E.
CITEPA, 2018. Inventaire des émissions de polluants atmosphériques en France au titre de la convention sur la pollution atmosphérique transfrontalière à longue distance et de la directive européenne concernant la réduction des émissions nationales de certains polluants.
Council of the EU, 2024. Euro 7: council adopts new rules on emission limits for cars, vans and trucks.
Daellenbach, K.R., Uzu, G., Jiang, J., Cassagnes, L.-E., Leni, Z., Vlachou, A., Stefenelli, G., Canonaco, F., Weber, S., Segers, A., Kuenen, J.J.P., Schaap, M., Favez, O., Albinet, A., Aksoyoglu, S., Dommen, J., Baltensperger, U., Geiser, M., El Haddad, I., Jaffrezo, J.-L., Prévôt, A.S.H., 2020. Sources of particulate-matter air pollution and its oxidative potential in Europe. Nature 587, 414–419. https://doi.org/10.1038/s41586-020-2902-8.
de Hoogh, K., Chen, J., Gulliver, J., Hoffmann, B., Hertel, O., Ketzel, M., Bauwelinck, M., van Donkelaar, A., Hvidtfeldt, U.A., Katsouyanni, K., Klompmaker, J., Martin, R.V., Samoli, E., Schwartz, P.E., Stafoggia, M., Bellander, T., Strak, M., Wolf, K., Vienneau, D., Brunekreef, B., Hoek, G., 2018. Spatial PM2.5, NO2, O3 and BC models for Western Europe – evaluation of spatiotemporal stability. Environ. Int. 120, 81–92. https://doi.org/10.1016/j.envint.2018.07.036.
Denier van der Gon, H.A.C., Hulskotte, J.H.J., Visschedijk, A.J.H., Schaap, M., 2007. A revised estimate of copper emissions from road transport in UNECE-Europe and its impact on predicted copper concentrations. Atmos. Environ. 41, 8697–8710. https://doi.org/10.1016/j.atmosenv.2007.07.033.
Denier van der Gon, H., Hulskotte, J., Jozwicka, M., Kranenburg, R., Kuenen, J., Visschedijk, A., 2018. Chapter 5 – European emission inventories and projections for road transport non-exhaust emissions: analysis of consistency and gaps in emission inventories from EU member states. In: Amato, F. (Ed.), Non-Exhaust Emissions. Academic Press, pp. 101–121. https://doi.org/10.1016/B978-0-12-811770-5.00005-4.
Duncan, B.N., Lamsal, L.N., Thompson, A.M., Yoshida, Y., Lu, Z., Streets, D.G., Hurwitz, M.M., Pickering, K.E., 2016. A space-based, high-resolution view of notable changes in urban NOx pollution around the world (2005–2014). J. Geophys. Res. Atmos. 121, 976–996. https://doi.org/10.1002/2015JD024121.
EEA-Report, 2024. European Union emission inventory report 1990–2022.
El Haddad, I., Vienneau, D., Daellenbach, K.R., Modini, R., Slowik, J.G., Upadhyay, A., Vasilakos, P.N., Bell, D., de Hoogh, K., Prevot, A.S.H., 2024. Opinion: how will advances in aerosol science inform our understanding of the health impacts of outdoor particulate pollution? Atmos. Chem. Phys. 24, 11981–12011. https://doi.org/10.5194/acp-24-11981-2024.
EMISIA, 2020. COPERT data, emissions from road transport for 31 European countries, received 10 Nov 2020.
European Union, 1999. The European Commission bans White Asbestos.
Fussell, J.C., Franklin, M., Green, D.C., Gustafsson, M., Harrison, R.M., Hicks, W., Kelly, F.J., Kishta, F., Miller, M.R., Mudway, I.S., Oroumiyeh, F., Selley, L., Wang, M., Zhu, Y., 2022. A review of road traffic-derived non-exhaust particles: emissions, physicochemical characteristics, health risks, and mitigation measures. Environ. Sci. Technol. 56, 6813–6835. https://doi.org/10.1021/acs.est.2c01072.
Galli, T.T., de Campos, E.C., do Nascimento Camargo, L., Fukuzaki, S., dos Santos, T.M., Hamaguchi, S.S.S., Bezerra, S.K.M., Silva, F.J.A., Rezende, B.G., dos Santos Lopes, F. T.Q., Olivo, C.R., Saraiva-Romanholo, B.M., Prado, C.M., Leick, E.A., Bourotte, C.L. M., Benseñor, I.J.M., Lotufo, P.A., Righetti, R.F., Tibério, I.F.L.C., 2024. Effects of environmental exposure to iron powder on healthy and elastase-exposed mice. Sci. Rep. 14, 9134. https://doi.org/10.1038/s41598-024-59573-8.
Gini, M., Manousakas, M.-I., Kantarelou, V., Karydas, A.-G., Chiari, M., Migliori, A., Civici, N., Veleva, B., Šega, K., Samek, L., Samara, C., Kertesz, Z., Osan, J., Eleftheriadis, K., 2021. Inter-laboratory comparison of ED-XRF/PIXE analytical techniques in the elemental analysis of filter-deposited multi-elemental certified reference materials representative of ambient particulate matter. Sci. Total Environ. 780, 146449. https://doi.org/10.1016/j.scitotenv.2021.146449.
Gon, H.A.C.D. Van Der, Gerlofs-nijland, M.E., Gehrig, R., Gustafsson, M., Janssen, N., Harrison, R.M., Hulskotte, J., Jozwicka, M., Keuken, M., Krijgsheld, K., Ntziachristos, L., Riediker, M., Cassee, F.R., Gustafsson, M., Janssen, N., Harrison, R.M., Hulskotte, J., Johansson, C., Jozwicka, M., Keuken, M., Krijgsheld, K., Ntziachristos, L., Riediker, M., Gon, H.A.C.D. Van Der, Gerlofs-nijland, M.E., Gehrig, R., Gustafsson, M., Janssen, N., Harrison, R.M., Hulskotte, J., Johansson, C., Jozwicka, M., Keuken, M., Krijgsheld, K., Ntziachristos, L., 2013. The policy relevance of wear emissions from road transport, now and in the future—an international workshop report and consensus statement 2247. Doi: 10.1080/10962247.2012.741055.
Grange, S.K., Carslaw, D.C., Lewis, A.C., Boleti, E., Hueglin, C., 2018. Random forest meteorological normalisation models for Swiss chem{PM_{10}} trend analysis. Atmos. Chem. Phys. 18, 6223–6239. https://doi.org/10.5194/acp-18-6223-2018.
Hampel, R., Peters, A., Beelen, R., Brunekreef, B., Cyrys, J., de Faire, U., de Hoogh, K., Fuks, K., Hoffmann, B., Hüls, A., Imboden, M., Jedynska, A., Kooter, I., Koenig, W., Künzli, N., Leander, K., Magnusson, P., Männistö, S., Penell, J., Pershagen, G., Phuleria, H., Probst-Hensch, N., Pundt, N., Schaffner, E., Schikowski, T., Sugiri, D., Tiittanen, P., Tsai, M.-Y., Wang, M., Wolf, K., Lanki, T., 2015. Long-term effects of elemental composition of particulate matter on inflammatory blood markers in European cohorts. Environ. Int. 82, 76–84. https://doi.org/10.1016/j.envint.2015.05.008.
Han, T., Hu, X., Zhang, J., Xue, W., Che, Y., Deng, X., Zhou, L., 2023. Rebuilding high-quality near-surface ozone data based on the combination of WRF-Chem model with a machine learning method to better estimate its impact on crop yields in the Beijing-Tianjin-Hebei region from 2014 to 2019. Environ. Pollut. 336, 122334. https://doi.org/10.1016/j.envpol.2023.122334.
Harrison, R.M., Allan, J., Carruthers, D., Heal, M.R., Lewis, A.C., Marner, B., Murrells, T., Williams, A., 2021. Non-exhaust vehicle emissions of particulate matter and VOC from road traffic: a review. Atmos. Environ. 262, 118592. https://doi.org/10.1016/j.atmosenv.2021.118592.
Hosseinpour, F., Kumar, N., Tran, T., Knipping, E., 2024. Using machine learning to improve the estimate of U.S. background ozone. Atmos. Environ. 316, 120145. https://doi.org/10.1016/j.atmosenv.2023.120145.
Hu, X., Belle, J.H., Meng, X., Wildani, A., Waller, L.A., Strickland, M.J., Liu, Y., 2017. Estimating PM2.5 concentrations in the conterminous United States using the random forest approach. Environ. Sci. Technol. 51, 6936–6944. https://doi.org/10.1021/acs.est.7b01210.
Hulskotte, J.H.J., Roskam, G.D., Denier van der Gon, H.A.C., 2014. Elemental composition of current automotive braking materials and derived air emission factors. Atmos. Environ. 99, 436–445. https://doi.org/10.1016/j.atmosenv.2014.10.007.
Ivatt, P.D., Evans, M.J., 2020. Improving the prediction of an chemistry transport model using gradient-boosted regression treesatmospheric. Atmos. Chem. Phys. 20, 8063–8082. https://doi.org/10.5194/acp-20-8063-2020.
Jiang, J., Aksoyoglu, S., Ciarelli, G., Oikonomakis, E., El-Haddad, I., Canonaco, F., O'Dowd, C., Ovadnevaite, J., Minguillón, M.C., Baltensperger, U., Prévôt, A.S.H., 2019a. Effects of two different biogenic emission models on modelled ozone and aerosol concentrations in Europe. Atmos. Chem. Phys. 19, 3747–3768. https://doi.org/10.5194/acp-19-3747-2019.
Jiang, J., Aksoyoglu, S., El-Haddad, I., Ciarelli, G., van der Gon, H.A.C., Canonaco, F., Gilardoni, S., Paglione, M., Minguillón, M.C., Favez, O., Zhang, Y., Marchand, N., Hao, L., Virtanen, A., Florou, K., O'Dowd, C., Ovadnevaite, J., Baltensperger, U., Prévôt, A.S.H., 2019b. Sources of organic aerosols in Europe: a modeling study using CAMx with modified volatility basis set scheme. Atmos. Chem. Phys. 19, 15247–15270. https://doi.org/10.5194/acp-19-15247-2019.
Jianyao, Y., Yuan, H., Su, G., Wang, J., Weng, W., Zhang, X., 2025. Machine learning-enhanced high-resolution exposure assessment of ultrafine particles. Nat. Commun. 16, 1209. https://doi.org/10.1038/s41467-025-56581-8.
Johansson, C., Norman, M., Burman, L., 2009. Road traffic emission factors for heavy metals. Atmos. Environ. 43, 4681–4688. https://doi.org/10.1016/j.atmosenv.2008.10.024.
Kuenen, J., Dellaert, S., Visschedijk, A., Jalkanen, J.-P., Super, I., van der Gon, H., 2022. CAMS-REG-v4: a state-of-the-art high-resolution European emission inventory for air quality modelling. Earth Syst. Sci. Data 14, 491–515. https://doi.org/10.5194/essd-14-491-2022.
Lacima, A., Petetin, H., Soret, A., Bowdalo, D., Jorba, O., Chen, Z., Méndez Turrubiates, R.F., Achebak, H., Ballester, J., Pérez Garc'ia-Pando, C., 2023. Long-term evaluation of surface air pollution in CAMSRA and MERRA-2 global reanalyses over Europe (2003–2020). Geosci. Model Dev. 16, 2689–2718. https://doi.org/10.5194/gmd-16-2689-2023.
Lucarelli, F., Nava, S., Calzolai, G., Chiari, M., Udisti, R., Marino, F., 2011. Is PIXE still a useful technique for the analysis of atmospheric aerosols? The LABEC experience. X-Ray Spectrom. 40, 162–167. https://doi.org/10.1002/xrs.1312.
Masiol, M., Squizzato, S., Formenton, G., Harrison, R.M., Agostinelli, C., 2017. Air quality across a European hotspot: Spatial gradients, seasonality, diurnal cycles and

trends in the Veneto region, NE Italy. Sci. Total Environ. 576, 210–224. https://doi.org/10.1016/j.scitotenv.2016.10.042.
Monforti Ferrario, F., Crippa, M., Guizzardi, D., Muntean, M., Schaaf, E., Banja, M., Pagani, F., Solazzo, E., 2022. Global air pollutant emissions – EDGAR v6.1. Eur. Comm. Jt. Res. Cent.
Mues, A., Kuenen, J., Hendriks, C., Manders, A., Segers, A., Scholz, Y., Hueglin, C., Builtjes, P., Schaap, M., 2014. Sensitivity of air pollution simulations with LOTOS-EUROS to the temporal distribution of anthropogenic emissions. Atmos. Chem. Phys. 14, 939–955. https://doi.org/10.5194/acp-14-939-2014.
Panagos, P., Van Liedekerke, M., Borrelli, P., Köninger, J., Ballabio, C., Orgiazzi, A., Lugato, E., Liakos, L., Hervas, J., Jones, A., Montanarella, L., 2022. European soil data centre 2.0: soil data and knowledge in support of the EU policies. Eur. J. Soil Sci. 73, e13315. https://doi.org/10.1111/ejss.13315.
Pedregosa, F., Varoquaux, G., Gramfort, A., Michel, V., Thirion, B., 2011. Scikit-learn: machine learning in python. J. Mach. Learn. Res. 12, 2825–2830.
Reusser, J.E., 2023. Geochemical soil atlas of Switzerland distribution of 20 elements in the topsoil. Agroscope, 8046 Zurich, Switz. Doi: 10.34776/gca23-e.
Rodopoulou, S., Stafoggia, M., Chen, J., de Hoogh, K., Bauwelinck, M., Mehta, A.J., Klompmaker, J.O., Oftedal, B., Vienneau, D., Janssen, N.A.H., Strak, M., Andersen, Z.J., Renzi, M., Cesaroni, G., Nordheim, C.F., Bekkevold, T., Atkinson, R., Forastiere, F., Katsouyanni, K., Brunekreef, B., Samoli, E., Hoek, G., 2022. Long-term exposure to fine particle elemental components and mortality in Europe: results from six European administrative cohorts within the ELAPSE project. Sci. Total Environ. 809, 152205. https://doi.org/10.1016/j.scitotenv.2021.152205.
Saitoh, K., Sera, K., Gotoh, T., Nakamura, M., 2002. Comparison of elemental quantity by PIXE and ICP-MS and/or ICP-AES for NIST standards. Nucl. Instrum. Methods Phys. Res. Sect. B 189, 86–93. https://doi.org/10.1016/S0168-583X(01)01012-6.
Salma, I., Maenhaut, W., 2006. Changes in elemental composition and mass of atmospheric aerosol pollution between 1996 and 2002 in a Central European city. Environ. Pollut. 143, 479–488. https://doi.org/10.1016/j.envpol.2005.11.042.
Sayeed, A., Eslami, E., Lops, Y., Choi, Y., 2022. CMAQ-CNN: a new-generation of post-processing techniques for chemical transport models using deep neural networks. Atmos. Environ. 273, 118961. https://doi.org/10.1016/j.atmosenv.2022.118961.
Schaap, M., Kranenburg, R., Curier, L., Jozwicka, M., Dammers, E., Timmermans, R., 2013. Assessing the sensitivity of the OMI-NO2 product to emission changes across Europe. Remote Sens. 5, 4187–4208. https://doi.org/10.3390/rs5094187.
Schiavo, B., Meza-Figueroa, D., Vizuete-Jaramillo, E., Robles-Morua, A., Angulo-Molina, A., Reyes-Castro, P.A., Inguaggiato, C., Gonzalez-Grijalva, B., Pedroza-Montero, M., 2023. Oxidative potential of metal-polluted urban dust as a potential environmental stressor for chronic diseases. Environ. Geochem. Health 45, 3229–3250. https://doi.org/10.1007/s10653-022-01403-9.
Thorpe, A., Harrison, R.M., 2008. Sources and properties of non-exhaust particulate matter from road traffic: a review. Sci. Total Environ. 400, 270–282. https://doi.org/10.1016/j.scitotenv.2008.06.007.
Timmers, V.R.J.H., Achten, P.A.J., 2016. Non-exhaust PM emissions from electric vehicles. Atmos. Environ. 134, 10–17. https://doi.org/10.1016/j.atmosenv.2016.03.017.
Wong, P.-Y., Lee, H.-Y., Chen, Y.-C., Zeng, Y.-T., Chern, Y.-R., Chen, N.-T., Candice Lung, S.-C., Su, H.-J., Wu, C.-D., 2021. Using a land use regression model with machine learning to estimate ground level PM2.5. Environ. Pollut. 277, 116846. https://doi.org/10.1016/j.envpol.2021.116846.
Woo, S.-H., Jang, H., Lee, S.-B., Lee, S., 2022. Comparison of total PM emissions emitted from electric and internal combustion engine vehicles: an experimental analysis. Sci. Total Environ. 842, 156961. https://doi.org/10.1016/j.scitotenv.2022.156961.
Wu, H., Yang, T., Li, H., Zhou, Z., 2023. Air quality prediction model based on mRMR–RF feature selection and ISSA–LSTM. Sci. Rep. 13, 12825. https://doi.org/10.1038/s41598-023-39838-4.
Xu, M., Jin, J., Wang, G., Segers, A., Deng, T., Lin, H.X., 2021. Machine learning based bias correction for numerical chemical transport models. Atmos. Environ. 248, 118022. https://doi.org/10.1016/j.atmosenv.2020.118022.